Since January 2020 Elsevier has created a COVID-19 resource centre with free information in English and Mandarin on the novel coronavirus COVID-19. The COVID-19 resource centre is hosted on Elsevier Connect, the company's public news and information website.

Available online at www.sciencedirect.com
SCIENCE DIRECT
Virology 345 (2006) 337 – 345
VIROLOGY
www.elsevier.com/locate/yviro

Differential localization and turnover of infectious bronchitis virus 3b protein in mammalian versus avian cells

Amanda R. Pendleton, Carolyn E. Machamer *

Department of Cell Biology, Johns Hopkins University School of Medicine, 725 N. Wolfe St., Baltimore, MD 21205, USA

Received 27 July 2005; returned to author for revision 15 September 2005; accepted 22 September 2005
Available online 18 November 2005

Abstract

Infectious bronchitis virus (IBV) 3b protein is highly conserved among group 3 coronaviruses, suggesting that it is important for infection. A previous report (Virology 2003, 311:16–27) indicated that transfected IBV 3b localized to the nucleus in mammalian cells using a vaccinia-virus expression system. Although we confirmed these findings, we observed cytoplasmic localization of IBV 3b with apparent exclusion from the nucleus in avian cells (IBV normally infects chickens). IBV 3b was virtually undetectable by microscopy in mammalian cells transfected without vaccinia virus and in IBV-infected mammalian cells because of a greatly reduced half-life in these cells. A proteasome inhibitor stabilized IBV 3b in mammalian cells, but had little effect on IBV 3b in avian cells, suggesting that rapid turnover of IBV 3b in mammalian cells is proteasome-dependent while turnover in avian cells may be proteasome-independent. Our results highlight the importance of using cells derived from the natural host when studying coronavirus non-structural proteins.

Keywords: Infectious bronchitis virus; Accessory protein; IBV 3b; Protein degradation; Ubiquitin; Proteasome

Introduction

Members of the *Coronaviridae* family have large, positive-sense, single stranded RNA genomes (reviewed in Navas-Martin and Weiss, 2004). During infection, four structural proteins are expressed: spike (S), membrane (M), nucleocapsid (N), and envelope (E). Interestingly, several other open reading frames (ORFs) between the structural protein ORFs produce proteins of undetermined function during infection (Brown and Brierley, 1995). These proteins are thought to be non-structural, accessory proteins that are essential for productive viral infection in the natural host, but dispensable for virus growth in cell culture. For example, recombinant infectious bronchitis virus (IBV) lacking the IBV 5a gene showed similar cytopathic effect (CPE), and growth kinetics when compared to wild-type virus in cell culture, although final titers were slightly lower (Youn et al., 2005). Another group reported comparable results for the IBV 5b gene (Casais et al., 2005). A recent study showed the emergence of a mutant IBV following 36 passages in Vero cells that contained a C-terminally truncated version of IBV 3b (Shen et al., 2003). This result indicated that full-length IBV 3b is not essential for virus replication in Vero cells. Infectious clones of murine hepatitis virus (MHV) lacking the MHV 2a gene and/or the MHV 4 and MHV 5a genes showed CPE and growth kinetics that mirrored wild-type virus in cultured cells, although final titers were 10-fold lower in virus lacking the MHV 4 and MHV 5a genes (de Haan et al., 2002). Significantly, MHV lacking these genes showed attenuated infection in the natural host. Similar attenuation of infection by deletion of coronavirus accessory proteins has been reported for feline infectious peritonitis virus (Haijema et al., 2004) and transmissible gastroenteritis virus (Curtis et al., 2002; Ortego et al., 2003; Sola et al., 2003). Recently, more attention has been paid to coronavirus accessory proteins following the implication of a newly discovered coronavirus as a human pathogen in severe acute respiratory syndrome (SARS) (reviewed in Tan et al., 2005). Study of these accessory proteins will help more fully elucidate pathogenesis mechanisms and may lead to the development of more effective antiviral drugs.

IBV, a group 3 coronavirus, produces two non-structural proteins, 3a and 3b, from ORFs located between the S and E

* Corresponding author. Fax: +1 410 955 4129.
E-mail address: machamer@jhmi.edu (C.E. Machamer).

0042-6822/$ - see front matter © 2005 Elsevier Inc. All rights reserved.
doi:10.1016/j.virol.2005.09.069

genes (Liu et al., 1991). Both of these proteins are translated from subgenomic mRNA 3, with IBV 3a translation initiated via the first AUG, and the downstream IBV 3b translation initiated via leaky ribosomal scanning (Liu and Inglis, 1992). Subgenomic mRNA 3 also produces the IBV E protein through an internal ribosomal entry site. The amino acid sequences of the IBV 3a and IBV 3b proteins are highly conserved (81 to 86.2% similarity for IBV 3a and 87.5 to 95.4% for IBV 3b) among group 3 field isolates from different continents and decades (Jia and Naqi, 1997), suggesting that these proteins are essential for infection of the natural host. We have been studying the cell biology of the IBV 3a and 3b proteins to understand their functions. Previously, we reported that a pool of IBV 3a is tightly associated with membranes (Pendleton and Machamer, 2005). This membrane-associated pool of IBV 3a was localized in puncta at a novel domain of the smooth endoplasmic reticulum, suggesting that it may modulate cellular events occurring in this location. Another group recently reported that transiently expressed, full-length IBV 3b is localized to the nucleus in mammalian cells infected with vaccinia virus, while a C-terminally truncated form localized to the both the cytoplasm and the nucleus (Shen et al., 2003). This report was the first showing a non-essential, non-structural coronavirus protein localized to the nucleus. Additionally, recent reports have demonstrated that SARS 3b, which shares no homology with IBV 3b but is translated from the same genomic region, localizes to the nucleus when transiently expressed (Yuan et al., in press).

Here, we confirm that IBV 3b localizes to the nucleus when transiently expressed in vaccinia virus-infected mammalian cells. However, our findings show that the localization of IBV 3b in IBV-infected avian cells is cytoplasmic with apparent exclusion from the nucleus. Transient expression of IBV 3b without the use of vaccinia virus gave a similar cytoplasmic localization pattern in avian cells. Interestingly, IBV 3b protein expression was significantly lower in all mammalian cells tested when compared to avian cells. This reduction resulted from increased turnover of IBV 3b in mammalian cells that was mediated by the proteasome without the ubiquitylation of the sole lysine residue in IBV 3b. In contrast, the turnover of IBV 3b in avian cells was unaffected by a proteasome inhibitor, suggesting that it may be proteasome-independent. These results have implications for the study of non-structural coronavirus proteins, emphasizing the importance of using cells derived from the natural host when studying coronavirus accessory proteins.

Results

IBV 3b localization in mammalian and avian cells

IBV 3b is a small protein (63 amino acids) with no predicted structural motifs or domains. Glutathione *S*-transferase (GST) protein fused to the N-terminus of IBV 3b was expressed in bacteria, purified, and used to generate polyclonal antibodies to IBV 3b. Immunoprecipitation of in vitro translated IBV 3b was used to screen the antisera. Following SDS-PAGE, a clear band at approximately 6 kDa corresponding to in vitro translated IBV 3b was observed in samples immunoprecipitated with anti-IBV 3b antibodies (Fig. 1). No band was seen when in vitro translation reactions using an empty vector as template were immunoprecipitated. These results indicated that the antibodies were specific for IBV 3b (see also Fig. 3A).

Next, these antibodies were used to examine the intracellular localization of IBV 3b. Vero cells were infected with vTF7-3 (vaccinia virus expressing T7 RNA polymerase) followed by transfection at 1 h postinfection (p.i.) with a plasmid encoding IBV 3b driven by the T7 promoter. Analysis by indirect immunofluorescence microscopy at 6 h p.i. demonstrated that IBV 3b was localized mainly to the nucleus (Fig. 2A). Non-transfected cells on the same coverslip served as negative controls for antibody staining. Similar results were obtained in BHK-21 and HeLa cells (not shown). These findings are consistent with earlier studies (Shen et al., 2003). However, Vero cells transiently transfected without the use of vTF7-3 using a plasmid encoding IBV 3b expressed from the human cytomegalovirus immediate early promoter showed almost no IBV 3b staining (Fig. 2B). Inclusion of a plasmid encoding the green fluorescent protein (GFP) during transfection marked the transfected cells. In the very few cells that did show IBV 3b staining (approximately one cell per 100,000), variable localization patterns were seen. Interestingly, none of these cells showed the mainly nuclear localization pattern that was observed in vaccinia virus-infected cells. Similar results were seen in HeLa and COS-7 cells (not shown). Importantly, transiently transfected GFP was readily expressed in these cells

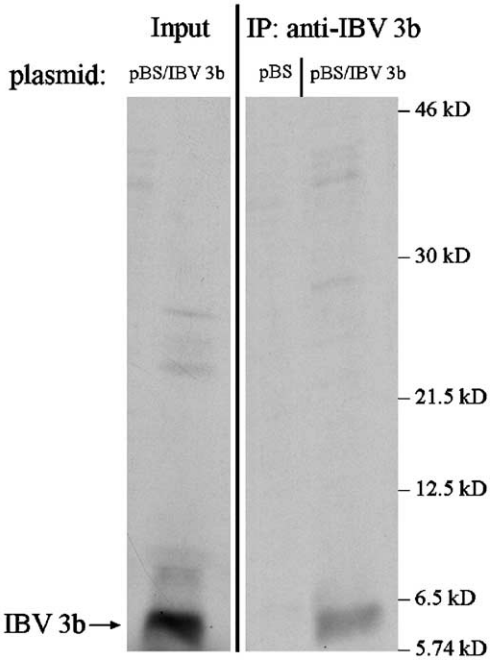

Fig. 1. Anti-IBV 3b antibodies are specific for IBV 3b. In vitro transcription/translation was performed using pBS (empty vector) and pBS/IBV 3b. Transcription/translation reactions were immunoprecipitated with anti-IBV 3b antibodies and visualized via SDS-PAGE. Input from the reaction that was not immunoprecipitated was used as a positive control.

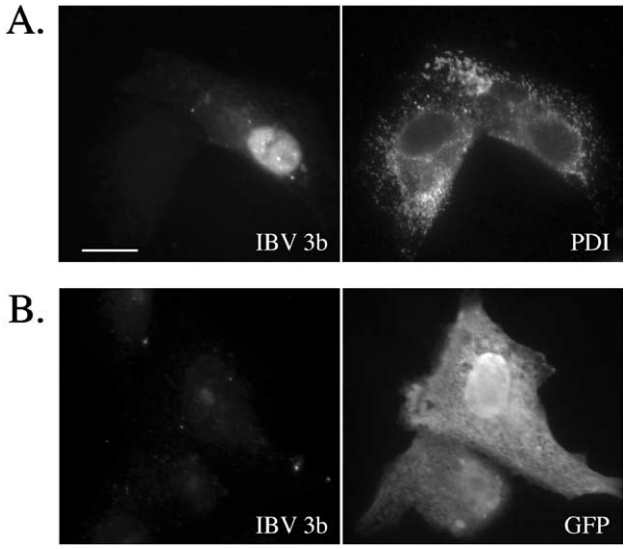

Fig. 2. IBV 3b localization in transiently transfected Vero cells. (A) vTF7-3-infected Vero cells were transiently transfected with pBS/IBV 3b at 1 h p.i. Cells were fixed and stained for indirect immunofluorescence at 6 h p.i. using anti-IBV 3b and anti-protein disulfide isomerase (PDI) antibodies. Scale bar, 15 μm. (B) Vero cells were transiently co-transfected with pEGFP-N1 (GFP-expressing vector) and pCMV/IBV 3b using Fugene 6. At 24 h posttransfection, cells were fixed and stained for indirect immunofluorescence with anti-IBV 3b and mouse anti-GFP antibodies.

(12.5% transfection efficiency) indicating that the lack of IBV 3b expression was not due to poor transfection. Transient transfection with a plasmid encoding tagged IBV 3b (pCMV/IBV 3b + G) followed by indirect immunofluorescence staining with antibodies to the G protein tag also showed virtually no IBV 3b staining (not shown). Therefore, the lack of IBV 3b staining did not result from a conformation or modification of IBV 3b that precluded recognition by anti-IBV 3b polyclonal antibodies. Finally, IBV 3b expression was undetectable in IBV-infected Vero cells by indirect immunofluorescence microscopy (not shown).

Because in vitro translated IBV 3b was readily detected by immunoprecipitation with anti-IBV 3b antibodies (Fig. 1), we hypothesized that the lack of IBV 3b expression by indirect immunofluorescence microscopy might be due to reduced IBV 3b protein levels in mammalian cells. Therefore, the presence of IBV 3b was assessed in cells derived from chickens, the natural IBV host. A clear band of the appropriate size for IBV 3b (approximately 6 kDa) was seen by immunoblotting of lysates from infected avian DF1 cells, but not mock-infected cells, again confirming IBV 3b antibody specificity (Fig. 3A). Additionally, transient transfection of DF1 cells with plasmids encoding IBV 3b and GFP (13.3% transfection efficiency) showed strong IBV 3b expression by indirect immunofluorescence microscopy. Intriguingly, IBV 3b was localized to the cytoplasm in these cells and appeared to be excluded from the nucleus (Fig. 3B), although more analytical techniques might be needed to definitively conclude that no IBV 3b is present in the nucleus. A similar IBV 3b localization pattern was observed in IBV-infected primary chicken embryo fibroblasts (CEFs) (Fig. 3C), IBV-infected DF1 cells (not shown), and DF1 cells transiently expressing a tagged version of IBV 3b (not shown). Thus, in contrast to results in mammalian cells, IBV 3b is readily visualized by indirect immunofluorescence microscopy in avian-derived cells.

IBV 3b is turned over more rapidly in Vero cells than in avian DF1 cells

To analyze the reduced IBV 3b expression in IBV-infected and plasmid-transfected mammalian cells, the half-life of IBV 3b was compared in mammalian and avian cells. IBV-infected Vero and DF1 cells were labeled with [^{35}S]-methionine–cysteine for 30 min. Cells were either harvested immediately (0 min chase time) or incubated in growth media for 15, 30, 45, or 60 min. Samples were divided in half with each half being immunoprecipitated by either anti-IBV 3b antibodies or anti-

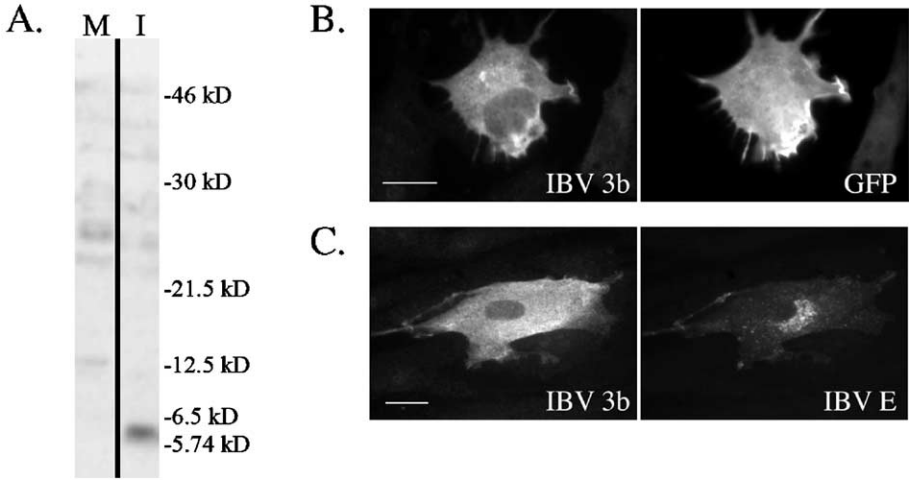

Fig. 3. IBV 3b localization in avian cells. (A) DF1 cells were infected with IBV (I) or mock-infected (M) as a negative control for 24 h. Cells were then lysed and visualized by immunoblotting using anti-IBV 3b antibodies. The figure shows one gel with both lanes at the same exposure level. (B) DF1 cells were transiently co-transfected with the pEGFP-N1 (GFP-expressing vector) and pCMV/IBV 3b plasmids. At approximately 24 h posttransfection, cells were fixed and stained for indirect immunofluorescence with anti-IBV 3b and mouse anti-GFP antibodies. Scale bar, 10 μm. (C) IBV-infected primary chicken embryo fibroblasts were fixed and stained for indirect immunofluorescence at 24 h p.i. using anti-IBV 3b and anti-IBV E antibodies. Scale bar, 15 μm.

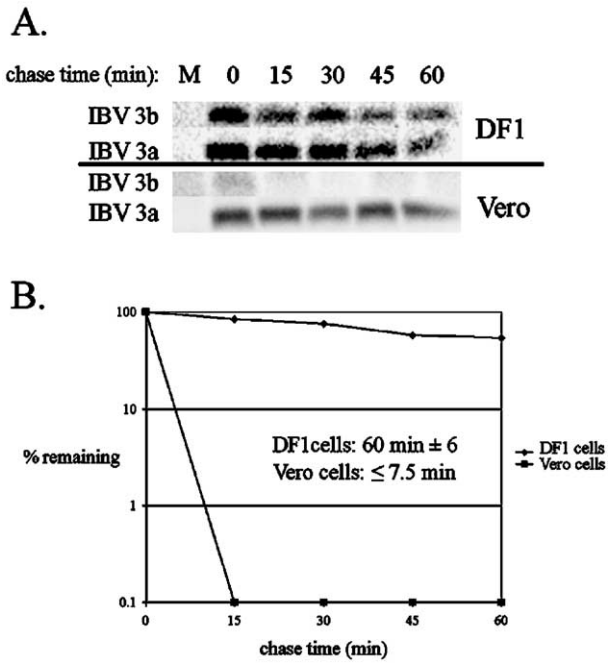

Fig. 4. IBV 3b is rapidly degraded in Vero cells. (A) IBV-infected DF1 or Vero cells were labeled at 24 h p.i. (DF1) or 12 h p.i. (Vero) for 30 min with [^{35}S]-methionine–cysteine followed by incubation in growth media for the chase times indicated. "M" denotes mock-infected cells. Samples were immunoprecipitated with anti-IBV 3b or anti-IBV 3a antibodies. (B) For each chase time, the graph shows the percent of original label seen at the 0 min chase that is remaining. Half-life calculations represent the average ± standard deviation of at least 3 experiments.

IBV 3a antibodies (as a control for infection) (Fig. 4A). Quantitation of SDS-PAGE gels from three experiments indicated that the half-life of IBV 3b was 60 min ± 6 min in DF1 cells while the half-life in Vero cells was ≤7.5 min (Fig. 4B). Half-life analysis of IBV 3b in DF1 and Vero cells transiently transfected with plasmids encoding IBV 3b gave similar results (not shown). Importantly, transient expression of a tagged version of IBV 3b (IBV 3b + G) followed by immunoprecipitation with antibodies to the protein tag also showed similar turnover rates in DF1 and Vero cells (not shown). These results confirmed that IBV 3b was not alternatively modified in Vero cells such that it became inaccessible to anti-IBV 3b antibodies. Thus, increased turnover of IBV 3b appeared to be responsible for its decreased expression in mammalian cells.

The turnover of IBV 3b is partially proteasome-dependent in Vero cells

To further assess the impact of turnover rates on IBV 3b expression in mammalian cells, Vero cells transiently transfected with plasmids encoding IBV 3b and GFP were treated for 4 h with the cell-permeable proteasome inhibitor, MG132, or DMSO as a control. During the final 25 min of MG132 treatment, cells were incubated in methionine–cysteine-free media (±MG132) for 15 min followed by labeling with [^{35}S]-methionine–cysteine (± MG132) for 10 min. Cells were then harvested and samples were split in half, with each half being immunoprecipitated with either anti-GFP antibodies (a control for transfection efficiency, not shown) or anti-IBV 3b antibodies. Results demonstrated a marked increase of IBV 3b levels in MG132-treated Vero cells, indicating proteasome involvement in the rapid rate of turnover of IBV 3b in Vero cells (Fig. 5A, lanes 1–4). IBV 3b expression was also readily detected by indirect immunofluorescence microscopy throughout the nucleus and cytoplasm under these same conditions (Fig. 5D). Surprisingly, treatment with MG132 did not cause significant accumulation of IBV 3b in DF1 cells (Fig. 5A, lanes 1–4). Also, the amount of IBV 3b remaining after a 60 min chase in the presence of MG132 was only marginally increased in DF1 cells (Fig. 5C, lanes 3–4). The level of ubiquitylated-actin was increased in MG132-treated DF1 cells, which served as a positive control (Fig. 5B). Interestingly, the amount of IBV 3b remaining after a 60 min chase in MG132-treated Vero cells (Fig. 5C, lanes 3–4) was similar to that seen in DF1cells (both treated and untreated) (Fig. 5C, lanes 1–4). These results suggest that a proteasome-independent mechanism may be primarily responsible for the degradation of IBV 3b in DF1 cells, and that a similar degradation method could be responsible for IBV 3b turnover in MG132-treated Vero cells.

Proteins are typically targeted for degradation *via* poly-ubiquitylation of lysine residues in the target protein. We mutated the single lysine residue in IBV 3b (Beaudette strain) to arginine (IBV 3b $K_{17}R$) to test the contribution of this lysine to IBV 3b turnover. Expression (Fig. 5A, lanes 5–7) and localization (not shown) of IBV 3b $K_{17}R$ in DF1 cells were similar to the wild-type protein. Vero cells were transiently transfected with plasmids encoding IBV 3b and GFP or IBV 3b $K_{17}R$ and GFP. Cells were incubated in methionine–cysteine-free media for 15 min followed by labeling in [^{35}S]-methionine–cysteine for 10 min. Samples were split in half and each half was immunoprecipitated with either anti-GFP antibodies (transfection control, not shown) or anti-IBV 3b antibodies. IBV 3b $K_{17}R$ was not stabilized relative to wild-type IBV 3b in Vero cells (Fig. 5A, lanes 5–7), indicating that the proteasome-mediated turnover of IBV 3b in mammalian cells did not depend on ubiquitylation of the IBV 3b lysine residue.

Discussion

IBV 3b is a highly conserved protein among group 3 coronaviruses (Jia and Naqi, 1997), suggesting it has a critical function in viral infection. Mammalian cells, particularly Vero cells, are frequently used to study IBV at the cellular level. However, our results have demonstrated significant differences in IBV 3b localization and turnover in mammalian cells when compared to avian cells. In chickens, IBV normally infects tracheal, bronchial, bursa, kidney, and chorioallentoic membrane epithelial cells, depending on the virus strain (Kapczynski et al., 2002; Naqi, 1990; Yagyu and Ohta, 1990). The mammalian cell lines used in this study were derived from either epithelial or fibroblast cells. The levels of expression and localization patterns in mammalian cells of

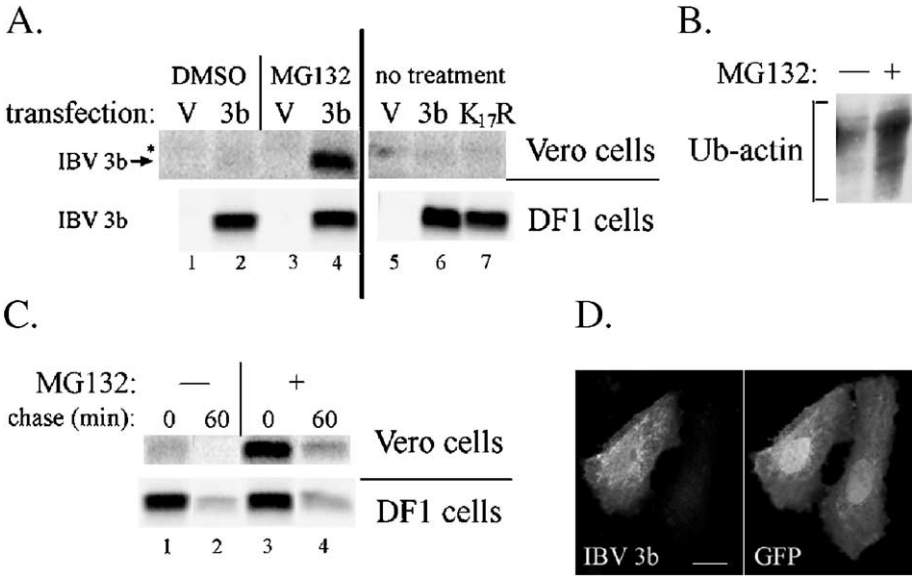

Fig. 5. Increased turnover of IBV 3b in Vero cells is mediated by the proteasome. (A) Vero and DF1 cells were transiently transfected with a total of 2 μg of DNA made up of one of the following combinations of plasmids: (a) pEGFP-N1 (GFP-expressing vector) and pCMV/IBV 3b (labeled "3b"), (b) pEGFP-N1 and pCMV/IBV 3b $K_{17}R$ (labeled "$K_{17}R$"), or (c) pEGFP-N1 alone (labeled "V"). At 24 h posttransfection, cells were treated with either (i) 50 μM MG132 (in DMSO) for 4 h, (ii) DMSO for 4 h, or (iii) no treatment. For the final 25 min of MG132 treatment, cells were incubated in serum-free medium lacking methionine and cysteine (±MG132/DMSO) for 15 min followed by labeling with [^{35}S]-methionine–cysteine (±MG132/DMSO) for 10 min. Samples were then immunoprecipitated with anti-IBV 3b antibodies or anti-GFP antibodies (not shown). The figure shows a single gel in which the lanes containing Vero cells have been transformed (using Quantity One software) so that the signal intensity shown is about 40 times more than the intensity shown in the DF1 cell lanes. * Denotes a background band. (B) Mock-transfected DF1 cells were treated with MG132 (labeled "+") or DMSO alone (labeled "−") without radiolabeling. Cells were then lysed and immunoprecipitated with anti-actin antibodies. Following SDS-PAGE, samples were immunoblotted with anti-ubiquitin antibodies and visualized by enhanced chemiluminescence. (C) Vero and DF1 cells were transiently transfected with pCMV/IBV 3b. At 24 h posttransfection, cells were radiolabeled and treated with MG132 or DMSO as described in panel A for 4 h. Cells were then incubated in regular growth medium (±MG132) for the chase times indicated. Immunoprecipitation with anti-IBV 3b antibodies followed. (D) Vero cells were transiently co-transfected with pEGFP-N1 and pCMV/IBV 3b. At 24 h posttransfection, cells were treated with MG132 for 4 h and fixed and stained for indirect immunofluorescence using anti-IBV 3b and anti-GFP antibodies. Scale bar, 15 μm.

either origin differed from those found in avian cells. Therefore, our results may point toward species specific differences in IBV 3b protein localization and turnover, suggesting that the study of this protein may be best accomplished in avian-derived cells.

One of the substantial differences observed in IBV 3b protein expression between avian and mammalian cells was that degradation of IBV 3b occurred much more rapidly in mammalian cells, resulting in almost undetectable levels of the protein by microscopy. This increased turnover of IBV 3b in mammalian cells (Fig. 4) was shown to be mediated by the proteasome while a proteasome-independent mechanism might be primarily responsible for the turnover of IBV 3b in avian cells (Fig. 5A). Interestingly, treatment of Vero cells with MG132 did not completely stabilize IBV 3b, but rather reduced its turnover rate to that found in avian cells. This result suggests that a proteasome-independent mechanism of turnover might be functional in both mammalian and avian cells, but that an additional proteasome-mediated degradation pathway for IBV 3b causes its extremely rapid turnover in Vero cells.

Proteasome-independent degradation has been described for several cytoplasmic proteins, including origin recognition complex 1B (ORC1B) protein, a DNA replication protein (Miyake et al., 2005), and IκBα, a specific inhibitor of NFκB (Shumway and Miyamoto, 2004). In the case of IκBα, a cytoplasmic protein that is constitutively and rapidly degraded by a proteasome-independent mechanism in certain B-lymphocytes, degradation was shown to be through the action of calcium/calmodulin-dependent proteases. An analogous mechanism through these or other proteases might function in proteasome-independent degradation of IBV 3b.

Intriguingly, when examining the additional proteasome-mediated turnover mechanism that is functional in Vero cells, we made the surprising discovery that mutating the one lysine in IBV 3b to arginine did not stabilize IBV 3b (Fig. 5A, lanes 5–7). Proteasome-dependent protein degradation is thought to occur primarily through the covalent addition of polyubiquitin to a lysine residue within the protein to be degraded. However, exceptions have been reported (reviewed in Ciechanover and Ben-Saadon, 2004; Hoyt and Coffino, 2004). For example, several proteins, including human papillomavirus and Epstein–Barr virus proteins, are polyubiquitylated at the amino-terminus (Aviel et al., 2000; Ikeda et al., 2002; Kuo et al., 2004; Reinstein et al., 2000). Also, a recent report showed that in cells infected with Kaposi's sarcoma-associated herpesvirus, a viral protein was able to polyubiquitylate cysteine residues of a cellular transmembrane protein, leading to degradation through the lysosomal pathway (Cadwell and Coscoy, 2005). For other proteins, such as the cell-cycle regulatory protein $p21^{Cip1}$, proteasomal degradation has been shown to be independent of ubiquitin addition; however, the specific

turnover mechanism remains controversial (Bloom et al., 2003; Chen et al., 2004; Sheaff et al., 2000). Also, ornithine decarboxylase (Zhang et al., 2003) and cyclin D1 (Newman et al., 2004) are targeted for proteasomal degradation by the non-covalent binding of antizyme, a protein that is recognized by the same domain of the proteasome that recognizes polyubiquitin. Any of these potential mechanisms might explain the observed proteasomal degradation of IBV 3b in mammalian cells that is independent of ubiquitin addition at Lys_{17}. The differences between avian and mammalian proteomes might allow recognition of IBV 3b by antizyme or the N-terminal ubiquitylation machinery in mammalian cells but not avian cells. Or, alternative posttranslational modification of IBV 3b in mammalian cells might cause these effects. Although SDS-PAGE did not show any differences in the electrophoretic mobility of IBV 3b in avian versus mammalian cells, more sensitive analytical methods might be needed to detect such differences. Additionally, IBV 3b may be protected from degradation by binding to a specific protein partner in avian cells that it is unable to bind in mammalian cells because of sequence differences or different posttranslation modifications. Given the small size of IBV 3b (~6 kDa) that would allow it to freely diffuse into the nucleus, the possible cytoplasmic retention of IBV 3b (Figs. 3B and C) suggests that such a scenario may be possible.

Interestingly, the increased turnover rate of IBV 3b might also explain the altered localization pattern of IBV 3b in vaccinia virus-infected mammalian cells when compared to transiently transfected or IBV-infected avian cells. Vaccinia virus infection of mammalian cells resulted in the localization of IBV 3b mainly to the nucleus (Fig. 2A). However, in avian cells, IBV 3b was localized to the cytoplasm with what may be nuclear exclusion (Figs. 3B and C). Additionally, in non-vTF7-3-infected Vero cells, IBV 3b was localized throughout the cytoplasm and nucleus upon treatment of cells with a proteasome inhibitor (Fig. 5D). Interestingly, one study indicated that proteasome-mediated, ubiquitin-independent turnover of $p21^{Cip1}$ was contingent on its localization: nuclear-localized $p21^{Cip1}$ was rapidly degraded while cytoplasmic $p21^{Cip1}$ was stable (Sheaff et al., 2000). Conversely, another cell-cycle regulatory protein, $p27^{Kip1}$, was stabilized in the nucleus while being quickly degraded when localized to the cytoplasm (Tomoda et al., 1999). Potentially, IBV 3b could be protected from degradation in the mammalian nucleus. This protection in conjunction with the massive amounts of IBV 3b produced by the robust vaccinia virus expression system might result in primarily nuclear IBV 3b in Vero cells if enough IBV 3b were able to reach the nucleus before being degraded. Alternatively, vaccinia virus infection might directly alter proteasome degradation of nuclear proteins or IBV 3b localization. Regardless, the vaccinia virus transfection system results in IBV 3b expression that is dissimilar to the more physiologically relevant expression found in IBV-infected avian and mammalian cells. Additionally, the lack of nuclear enrichment of IBV 3b during infection suggests that functional similarities between IBV 3b and nuclear localized SARS 3b are unlikely.

Finally, the differences in turnover of IBV 3b in mammalian versus avian cells have implications for functional and genetic studies of IBV 3b. One group recently reported the emergence of a C-terminally truncated version of IBV 3b following 36 passages in Vero cells (Shen et al., 2003). This study showed that full-length IBV 3b was not essential for virus replication in Vero cells, but did not rule out the possibility of an essential function for the N-terminus of the protein. However, the extremely short half-life of IBV 3b in Vero cells indicates that it is unlikely that any portion of IBV 3b is essential for viral replication in mammalian cell culture. Future studies using an infectious clone lacking IBV 3b will determine if IBV 3b is also dispensable for virus replication in avian cells. Finally, the IBV 3b protein in some strains of IBV lacks lysines. However, the proteasome-mediated degradation of IBV 3b in mammalian cells is not dependent on lysine ubiquitylation, suggesting that IBV 3b from any strain of IBV would need to be studied in avian systems. The results presented here document significant differences in localization and turnover of the IBV 3b accessory protein in different cell culture systems, thus suggesting the importance of using cells derived from the natural host when studying coronavirus accessory proteins.

Materials and methods

Cells and viruses

HeLa (human cervical epithelial), BHK-21 (baby hamster kidney fibroblast), COS7 (African green monkey kidney fibroblast-like), and UMNSAH/DF1 (DF1) (immortalized chicken embryo fibroblast) cells were maintained in high-glucose Dulbecco's modified Eagle's medium (DMEM) (Invitrogen Life Technologies, Carlsbad, CA) supplemented with 10% fetal calf serum (Atlanta Biologicals, Norcross, GA) and 0.1 mg/ml Normocin (Invivogen, San Diego, CA). Vero (African green monkey kidney epithelial) cells were maintained in DMEM supplemented with 5% fetal calf serum and Normocin. Primary chicken embryo fibroblasts (CEF) were a gift from Dr. K. Beemon (Johns Hopkins University, Baltimore, MD). Fibroblasts were maintained in Media 199 (Invitrogen) supplemented with 1% heat-inactivated chicken serum (Invitrogen), 1% fetal bovine serum (Invitrogen), and 2% tryptose phosphate (Sigma–Aldrich Co., St. Louis, MO). The previously described Vero-adapted Beaudette strain of IBV (Machamer and Rose, 1987) was used in all experiments with IBV-infected Vero cells. The egg-adapted strain of IBV (American Type Tissue Culture VR-22) was used in all experiments with IBV-infected DF1 cells and CEF cells. A vaccinia virus encoding T7 RNA polymerase (vTF7-3) was obtained from Bernard Moss (National Institutes of Health, Bethesda, MD) (Fuerst et al., 1986).

Plasmids

The IBV 3b gene was cloned by reverse transcription-PCR of mRNA isolated from IBV-infected Vero cells as described previously (Pendleton and Machamer, 2005). Briefly, primers

containing an *Eco*RI restriction site 5′ of the coding region of IBV 3b and a *Bam*HI restriction site behind the stop codon of IBV 3b were used to amplify the IBV 3b gene. These two restriction sites were then used to clone IBV 3b into pBluescript SK (pBS) (Stratagene, La Jolla, CA) behind the T7 promoter. Dideoxy sequencing confirmed that the IBV 3b sequence in this construct (called pBS/IBV 3b) matched the known IBV 3b Beaudette strain sequence (Liu et al., 1991). PCR amplification of pBS/IBV 3b with the same *Eco*RI-containing 5′ primer and a 3′ primer containing a *Not*I restriction site was performed to clone IBV 3b in frame with the C-terminal tail of the vesicular stomatitis virus G (VSV-G) protein (The C-terminal tail of the VSV-G protein had previously been inserted into the pBS plasmid using RT-PCR). This plasmid was named pBS/IBV 3b + G. IBV 3b + G was then subcloned into the pEGFP-N1 plasmid (BD Biosciences Clontech, San Diego, CA) using the *Eco*RI and *Xba*I restriction sites. A stop codon followed the IBV 3b + G reading frame so that the GFP protein was not expressed. This plasmid was named pCMV/IBV 3b + G. A plasmid encoding IBV 3b with the lysine$_{17}$ codon mutated to that for arginine was generated using QuikChange mutagenesis (Stratagene, La Jolla, CA) on the pBS/IBV 3b plasmid according to the manufacturer's protocol. The resulting plasmid was named pBS/IBV 3b $K_{17}R$. pBS/IBV 3b and pBS/IBV 3b $K_{17}R$ were used to subclone IBV 3b and IBV 3b $K_{17}R$ into the pEGFP-N1 plasmid with the *Eco*RI and *Bam*HI restriction enzymes. Again, stop codons were located at the end of the IBV 3b and IBV 3b $K_{17}R$ ORFs. Thus, GFP was not expressed from these plasmids. These plasmids were named pCMV/IBV 3b and pCMV/IBV 3b $K_{17}R$. PCR amplification was performed on the pBS/IBV 3b plasmid with primers containing *Bam*HI (5′) and *Eco*RI (3′) sites to clone IBV 3b into pGEX-2T (Amersham Pharmacia Biotech, Inc., Piscataway, NJ). The resulting plasmid, which contained the glutathione *S*-transferase (GST) protein fused to the N-terminus of IBV 3b, was named pGEX-2T/IBV 3b.

Fusion protein expression

The GST Gene Fusion System (Amersham) was used to express and purify the GST-IBV 3b fusion protein. Briefly, BL21 *Escherichia coli* bacteria were transformed with either the pGEX-2T/IBV 3b plasmid or pGEX-2T. Individual bacterial colonies were picked and grown overnight in YT broth (0.8% BactoTryptone (BD Biosciences, San Diego, CA), 1% Bacto yeast extract (BD Biosciences), 0.5% NaCl (Sigma)) containing 80 μg/ml ampicillin (Sigma). The next day, cultures were diluted 1:10 and grown to an OD_{600} of approximately 0.6. GST-IBV 3b and GST protein expression was then induced by growing cultures in 0.1 mM (final concentration) isopropyl-β-D-thiogalactopyranoside (Amersham) for 2 days at 13.5 °C. Cultures were pelleted by centrifugation at 20,800 × *g* for 1 min and resuspended in phosphate-buffered saline (Sigma) plus protease inhibitors (Sigma, catalog number P8340). Following sonication and pelleting of the cellular debris, soluble protein was bound to Glutathione Sepharose 4B (Amersham) overnight at 4 °C. Beads were then washed three times with PBS plus protease inhibitors at 4 °C followed by elution (two times) of protein at 4 °C in a solution containing 10 mM reduced glutathione (Sigma) and 50 mM Tris–HCl (Sigma) [pH 8]. SDS-PAGE analysis combined with Coomassie staining was used to assess purity and yield of GST-IBV 3b.

Antibodies

Purified GST-IBV 3b protein was used to create polyclonal antibodies in rabbits (Covance Research Products Inc., Denver, PA). Initially, the ability of anti-IBV 3b antibodies to recognize the IBV 3b protein was assessed using an in vitro TNT quick coupled transcription/translation T7 system (Promega Corporation, Madison, WI) according to the manufacturer's protocol. Briefly, pBS (empty vector) or pBS/IBV 3b was incubated for 90 min at 30 °C in a transcription/translation master mix containing [^{35}S]-Redivue–methionine (Amersham). Samples were then diluted in a detergent solution containing 62.5 mM EDTA (J.T. Baker, Phillipsburg, NJ), 50 mM Tris–HCl [pH 8], 0.4% deoxycholic acid (CalBiochem, La Jolla, CA), and 1% nonidet P40 substitute (Fluka Chemie AG, Buchs, Switzerland) plus protease inhibitors and immunoprecipitated with anti-IBV 3b antibodies. Immunoprecipitations were analyzed by SDS-PAGE and fluorography. Input from the in vitro translated reaction that had not been immunoprecipitated was used as a positive control.

Mouse anti-GFP antibodies used in indirect immunofluorescence microscopy were from Roche Molecular Biochemicals (Indianapolis, IN). Rabbit anti-GFP antibodies used in immunoprecipitation assays and Alexa-488-conjugated donkey anti-mouse immunoglobulin (IgG) were from Molecular Probes, Inc. (Eugene, OR). Texas red-conjugated donkey anti-rabbit IgG was obtained from Jackson ImmunoResearch Laboratories, Inc. (West Grove, PA). Mouse anti-protein disulfide isomerase antibodies, which label the endoplasmic reticulum, were from Stressgen Biotechnologies, Inc. (San Diego, CA). The rat polyclonal anti-IBV E antibody was described previously (Corse and Machamer, 2000). Rabbit polyclonal antibodies to the C-terminus of the vesicular stomatitis virus G protein were also described previously (Swift and Machamer, 1991). Mouse anti-actin antibodies were from ICN Biomedicals, Inc. (Aurora, OH). Affinity-purified rabbit anti-ubiquitin antibodies were a generous gift from Dr. Cecile Pickart (Johns Hopkins University School of Public Health, Baltimore, MD).

Infection and transient transfection

IBV infection was performed at a multiplicity of infection (MOI) of ~1 by allowing virus to absorb to cells in a small volume of serum-free DMEM for 1 h at 37 °C. Cells were then transferred to DMEM supplemented with 2% fetal calf serum and antibiotics. Infection with vTF7-3 was performed as previously described (Corse and Machamer, 2000) in serum-free DMEM. At 1 h postinfection (p.i.), vTF7-3-infected cells were transfected with 2 μg DNA per 35-mm dish and 6 μl of Fugene 6 (Roche) for 5 h. Transient transfection was performed by adding 2 μg DNA per 35-mm dish for approximately 24

h with 6 μl of Fugene 6. Plasmid-based transient transfection was performed without the use of vaccinia virus unless otherwise specified.

Indirect immunofluorescence microscopy

The method used for indirect immunofluorescence microscopy has been described previously (Corse and Machamer, 2000). Briefly, cells were fixed with 3% paraformaldehyde (Sigma) in phosphate-buffered saline for 10 min at room temperature. Permeabilization with 0.5% Triton X-100 (Sigma) for 3 min at room temperature followed. Cells were then stained with the appropriate primary and secondary antibodies. Images were taken on an Axioskop microscope (Zeiss, Thornwood, NY) at a magnification of 630× with an attached Sensys charge-coupled device camera (Photomerics, Tucson, AZ). IP Lab imaging software (Signal Analystics, Vienna, VA) was used to visualize images.

Immunoprecipitation and proteasome inhibitor treatment

Cells transiently transfected with pEGFP-N1 and either pCMV/IBV 3b or pCMV/IBV 3b $K_{17}R$ were incubated in serum-free media that lacked methionine and cysteine (Invitrogen) for 15 min before being labeled in [^{35}S]-methionine–cysteine (Promix; Amersham) for 10 min. Cells were then harvested in a detergent solution plus protease inhibitors (described above) and immunoprecipitated as previously described (Machamer and Rose, 1987). Quantitation of [^{35}S]-labeled protein was done by exposing SDS-PAGE gels to a K-HD imaging screen (Bio-Rad Laboratories, Hercules, CA) followed by scanning with personal molecular imager FX (Bio-Rad). Pixel intensity was determined with Quantity One software (Bio-Rad).

Half-lives of the IBV 3b or IBV 3b + G proteins were determined in infected or transiently transfected cells labeled with [^{35}S]-methionine–cysteine for 30 min. Cells were then either harvested immediately (0 min chase time) in detergent solution or incubated in normal growth medium for chase times of 15, 30, 45, or 60 min. Mock-infected cells were harvested immediately after labeling. Samples were immunoprecipitated and analyzed by SDS-PAGE and quantitated as described above. Half-lives were calculated by determining the formula (in the form $y = Ae^{bx}$) for the best-fit exponential curve when chase time (x) was graphed against pixel intensity (y). The half-life was equal to the x value when y was one-half the pixel intensity of the 0 min chase time.

For proteasome inhibitor treatment, transiently transfected cells were treated at approximately 24 h posttransfection with 50 μM MG132 (Sigma) for 4 h. During the final 25 min of treatment, cells were incubated in serum-free medium lacking methionine and cysteine (±MG132) for 15 min followed by labeling with [^{35}S]-methionine–cysteine (±MG132) for 10 min. Cells were then either harvested immediately or incubated with normal growth medium (±MG132) for 60 min. As a control, transfected cells were incubated in the same amount of DMSO solvent as the MG132-treated cells. Cell lysates were then immunoprecipitated, analyzed by SDS-PAGE, and quantitated as described above.

Immunoblotting

DF1 cells were infected for 24 h with IBV at a MOI of ~1 or mock-infected as a negative control. Cells were lysed in a solution containing 4% sodium dodecyl sulfate, 30% glycerol, 1% bromophenol blue, 10% 2-mercaptoethanol, and 0.1 M Tris–HCl (pH 8). Samples were then run on 17.5% SDS-PAGE gel and immunoblotted as described previously (Pendleton and Machamer, 2005). As a positive control for the efficacy of MG132 treatment in DF1 cells, mock-transfected cells were treated with MG132 for 4 h. Cells were then lysed without being radiolabeled and immunoprecipitated with anti-actin antibodies. Following SDS-PAGE, samples were immunoblotted with anti-ubiquitin antibodies.

Acknowledgments

This work was supported by National Institutes of Health grant GM64647.

We thank Emily Corse for the generation of the pBS/IBV 3b and pBS/IBV 3b+G plasmids, all members of the Machamer laboratory for helpful comments and stimulating discussion, Dr. Karen Beemon (Johns Hopkins University, Baltimore, MD) for the generous gift of primary chicken embryo fibroblasts, and Dr. Cecile Pickart (Johns Hopkins University School of Public Health, Baltimore, MD) for the generous gift of anti-ubiquitin antibodies and for helpful discussions.

References

Aviel, S., Winberg, G., Massucci, M., Ciechanover, A., 2000. Degradation of the epstein–barr virus latent membrane protein 1 (LMP1) by the ubiquitin–proteasome pathway. Targeting via ubiquitination of the N-terminal residue. J. Biol. Chem. 275 (31), 23491–23499.

Bloom, J., Amador, V., Bartolini, F., DeMartino, G., Pagano, M., 2003. Proteasome-mediated degradation of p21 via N-terminal ubiquitinylation. Cell 115 (1), 71–82.

Brown, T.D.K., Brierley, I., 1995. The coronavirus nonstructural proteins. In: Siddell, S.G. (Ed.), The Coronaviridae. Plenum Press, New York, pp. 191–217.

Cadwell, K., Coscoy, L., 2005. Ubiquitination on nonlysine residues by a viral E3 ubiquitin ligase. Science 309 (5731), 127–130.

Casais, R., Davies, M., Cavanagh, D., Britton, P., 2005. Gene 5 of the avian coronavirus infectious bronchitis virus is not essential for replication. J. Virol. 79 (13), 8065–8078.

Chen, X., Chi, Y., Bloecher, A., Aebersold, R., Clurman, B.E., Roberts, J.M., 2004. N-acetylation and ubiquitin-independent proteasomal degradation of p21 (Cip1). Mol. Cell 16 (5), 839–847.

Ciechanover, A., Ben-Saadon, R., 2004. N-terminal ubiquitination: more protein substrates join in. Trends Cell Biol. 14 (3), 103–106.

Corse, E., Machamer, C.E., 2000. Infectious bronchitis virus E protein is targeted to the Golgi complex and directs release of virus-like particles. J. Virol. 74 (9), 4319–4326.

Curtis, K.M., Yount, B., Baric, R.S., 2002. Heterologous gene expression from transmissible gastroenteritis virus replicon particles. J. Virol. 76 (3), 1422–1434.

de Haan, C.A., Masters, P.S., Shen, X., Weiss, S., Rottier, P.J., 2002. The group-specific murine coronavirus genes are not essential, but their

deletion, by reverse genetics, is attenuating in the natural host. Virology 296 (1), 177–189.
Fuerst, T.R., Niles, E.G., Studier, F.W., Moss, B., 1986. Eukaryotic transient-expression system based on recombinant vaccinia virus that synthesizes bacteriophage T7 RNA polymerase. Proc. Natl. Acad. Sci. U.S.A. 83 (21), 8122–8126.
Haijema, B.J., Volders, H., Rottier, P.J., 2004. Live, attenuated coronavirus vaccines through the directed deletion of group-specific genes provide protection against feline infectious peritonitis. J. Virol. 78 (8), 3863–3871.
Hoyt, M.A., Coffino, P., 2004. Ubiquitin-free routes into the proteasome. Cell. Mol. Life Sci. 61 (13), 1596–1600.
Ikeda, M., Ikeda, A., Longnecker, R., 2002. Lysine-independent ubiquitination of Epstein–Barr virus LMP2A. Virology 300 (1), 153–159.
Jia, W., Naqi, S.A., 1997. Sequence analysis of gene 3, gene 4 and gene 5 of avian infectious bronchitis virus strain CU-T2. Gene 189 (2), 189–193.
Kapczynski, D.R., Sellers, H.S., Rowland, G.N., Jackwood, M.W., 2002. Detection of in ovo-inoculated infectious bronchitis virus by immunohistochemistry and in situ hybridization with a riboprobe in epithelial cells of the lung and cloacal bursa. Avian Dis. 46 (3), 679–685.
Kuo, M.L., den Besten, W., Bertwistle, D., Roussel, M.F., Sherr, C.J., 2004. N-terminal polyubiquitination and degradation of the Arf tumor suppressor. Genes Dev. 18 (15), 1862–1874.
Liu, D.X., Inglis, S.C., 1992. Internal entry of ribosomes on a tricistronic mRNA encoded by infectious bronchitis virus. J. Virol. 66 (10), 6143–6154.
Liu, D.X., Cavanagh, D., Green, P., Inglis, S.C., 1991. A polycistronic mRNA specified by the coronavirus infectious bronchitis virus. Virology 184 (2), 531–544.
Machamer, C.E., Rose, J.K., 1987. A specific transmembrane domain of a coronavirus E1 glycoprotein is required for its retention in the Golgi region. J. Cell Biol. 105 (3), 1205–1214.
Miyake, Y., Mizuno, T., Yanagi, K., Hanaoka, F., 2005. Novel splicing variant of mouse Orc1 is deficient in nuclear translocation and resistant for proteasome-mediated degradation. J. Biol. Chem. 280 (13), 12643–12652 (Epub 2005 Jan 4).
Naqi, S.A., 1990. A monoclonal antibody-based immunoperoxidase procedure for rapid detection of infectious bronchitis virus in infected tissues. Avian Dis. 34 (4), 893–898.
Navas-Martin, S.R., Weiss, S., 2004. Coronavirus replication and pathogenesis: implications for the recent outbreak of severe acute respiratory syndrome (SARS), and the challenge for vaccine development. J. Neurovirol. 10 (2), 75–85.
Newman, R.M., Mobascher, A., Mangold, U., Koike, C., Diah, S., Schmidt, M., Finley, D., Zetter, B.R., 2004. Antizyme targets cyclin D1 for degradation. A novel mechanism for cell growth repression. J. Biol. Chem. 279 (40), 41504–41511.
Ortego, J., Sola, I., Almazan, F., Ceriani, J.E., Riquelme, C., Balasch, M., Plana, J., Enjuanes, L., 2003. Transmissible gastroenteritis coronavirus gene 7 is not essential but influences in vivo virus replication and virulence. Virology 308 (1), 13–22.
Pendleton, A.R., Machamer, C.E., 2005. Infectious bronchitis virus 3a protein localizes to a novel domain of the smooth endoplasmic reticulum. J. Virol. 79 (10), 6142–6151.
Reinstein, E., Scheffner, M., Oren, M., Ciechanover, A., Schwartz, A., 2000. Degradation of the E7 human papillomavirus oncoprotein by the ubiquitin–proteasome system: targeting via ubiquitination of the N-terminal residue. Oncogene 19 (51), 5944–5950.
Sheaff, R.J., Singer, J.D., Swanger, J., Smitherman, M., Roberts, J.M., Clurman, B.E., 2000. Proteasomal turnover of p21Cip1 does not require p21Cip1 ubiquitination. Mol. Cell 5 (2), 403–410.
Shen, S., Wen, Z.L., Liu, D.X., 2003. Emergence of a coronavirus infectious bronchitis virus mutant with a truncated 3b gene: functional characterization of the 3b protein in pathogenesis and replication. Virology 311 (1), 16–27.
Shumway, S.D., Miyamoto, S., 2004. A mechanistic insight into a proteasome-independent constitutive inhibitor kappaBalpha (IkappaBalpha) degradation and nuclear factor kappaB (NF-kappaB) activation pathway in WEHI-231 B-cells. Biochem. J. 380 (Pt 1), 173–180.
Sola, I., Alonso, S., Zuniga, S., Balasch, M., Plana-Duran, J., Enjuanes, L., 2003. Engineering the transmissible gastroenteritis virus genome as an expression vector inducing lactogenic immunity. J. Virol. 77 (7), 4357–4369.
Swift, A.M., Machamer, C.E., 1991. A Golgi retention signal in a membrane-spanning domain of coronavirus E1 protein. J. Cell Biol. 115 (1), 19–30.
Tan, Y.J., Lim, S.G., Hong, W., 2005. Characterization of viral proteins encoded by the SARS-coronavirus genome. Antivir. Res. 65 (2), 69–78.
Tomoda, K., Kubota, Y., Kato, J., 1999. Degradation of the cyclin-dependent-kinase inhibitor p27Kip1 is instigated by Jab1. Nature 398 (6723), 160–165.
Yagyu, K., Ohta, S., 1990. Detection of infectious bronchitis virus antigen from experimentally infected chickens by indirect immunofluorescent assay with monoclonal antibody. Avian Dis. 34 (2), 246–252.
Youn, S., Leibowitz, J.L., Collisson, E.W., 2005. In vitro assembled, recombinant infectious bronchitis viruses demonstrate that the 5a open reading frame is not essential for replication. Virology 332 (1), 206–215.
Yuan, X., Yao, Z., Shan, Y., Chen, B., Yang, Z., Wu, J., Zhao, Z., Chen, J., Cong, Y., in press. Nucleolar localization of non-structural protein 3b, a protein specifically encoded by the severe acute respiratory syndrome coronavirus. Virus Res.
Zhang, M., Pickart, C.M., Coffino, P., 2003. Determinants of proteasome recognition of ornithine decarboxylase, a ubiquitin-independent substrate. EMBO J. 22 (7), 1488–1496.